

SAR Processor based on a CFAR Signal or Interference Subspace Detector Matched to Man Made Target Detection in a Forest

Rémi DURAND *[†], Guillaume GINOLHAC [†], Laetitia THIRION *, Philippe FORSTER [†]

* SONDRRA / SUPELEC

3 rue Joliot Curie, Plateau du Moulon, 91192 Gif sur Yvette - FRANCE

Tel: +(00 33) 1 69 85 18 13

email: remi.durand@supelec.fr

[†] GEA - University Paris 10

PST Ville d'Avray, 92410 Ville d'Avray - FRANCE,

email: guillaume.ginolhac@u-paris10.fr

Abstract—This paper deals with two new SAR processors based on CFAR subspaces detector. These two algorithms aim at improving man made targets detection performances in a forest clutter by using electromagnetic scattering models. The implementation of the two detectors is described. An application on simulated data shows the interest of the two methods.

Index Terms: Detection, SAR, Subspace Detector, FOPEN, SAR processor.

I. INTRODUCTION

The detection of Man Made Targets (MMT) embedded in noise, clutter or speckle in SAR images is a current issue which concerns both SAR and signal processing communities. In a forest, it is possible to detect a MMT by using VHF-UHF (50 MHz to 1 GHz) waves to penetrate canopy. Unfortunately, at those frequencies, trunks remain high false alarm sources which must be treated, either by increasing the MMT response or by decreasing the forest clutter. In a previous paper [1], we focused on the first approach and proposed a new SAR processor. We demonstrated that classical SAR processors are detectors matched to isotropic points. These algorithms clearly do not use targets scattering properties. Assuming that MMT are single or set of canonical elements (eg. plates) with unknown orientations, we developed a subspace detector matched to these canonical elements responses and included it into the SAR processing. The processor obtained was called Subspace Detector SAR (SDSAR) algorithm (or quite recently Signal Subspace Detector SAR (SSDSAR) algorithm). We simulated a simple MMT and computed SSDSAR algorithm performance in a white Gaussian noise [2] and in a simulated trunk forest. The improvements obtained in terms of detection performance validated our approach. Some additional optimizations were developed to lower the computation task [3]. The SSDSAR algorithm only focused on improving the detection probability of the target by making assumptions on its scattering properties. The medium was considered to be a white Gaussian noise.

Although performances obtained were very encouraging when detecting a MMT in a simulated trunk forest [2] [3], the SSDSAR algorithm can be further improved by modelling more accurately the clutter of interest: the forest. We set two detection hypotheses: one sets that the signal scattered at a given position is the sum of a white Gaussian noise plus interferences generated by trunks, the other sets that the signal scattered is the sum of a white Gaussian noise plus the MMT response. We develop a CFAR version of the Generalized Likelihood Ratio Test (GLRT) to solve this problem and include it into the SAR processing. The SAR processor obtained is called Signal or Interference Subspace Detector SAR (SISDSAR) processor. This paper falls into three sections: in a first part, we present a new CFAR version of the algorithm which allows us to ignore the noise variance. The second part the SISDSAR algorithm detection problem and its GLRT. The last part compares performances obtained by CSAR, SSDSAR and SISDSAR algorithms when detecting a simple MMT embedded in a simulated forest.

The following conventions are adopted: italic indicates scalar quantity, lower case boldface indicates a vector quantity and upper case boldface matrix. T denotes the transpose operator and † the transpose conjugate. $CN(\mathbf{m}, \mathbf{R})$ denotes the complex Gaussian distribution with mean \mathbf{m} and covariance matrix \mathbf{R} .

II. THE SIGNAL SUBSPACE DETECTOR SAR (SSDSAR) ALGORITHM

A. Configuration

We consider a strip map SAR configuration: an airborne antenna is moving along an axis u . A signal $e(t)$ is emitted towards the scene at every u_i position of the antenna. The distance between two successive positions is δu . The received signal (raw data) at every u_i position is $z_i(t)$. We make the “stop and go” assumption: the antenna is not moving when emitting and receiving. \mathbf{e} and \mathbf{z}_i denote the vectors of signal samples associated to $e(t)$ and $z_i(t)$. Let

\mathbf{z} be the concatenation of n vertical vectors \mathbf{z}_i :

$$\mathbf{z} \in \mathbb{C}^M, \quad \mathbf{z} = [\mathbf{z}_1^T \quad \mathbf{z}_2^T \quad \dots \quad \mathbf{z}_n^T]^T \quad (1)$$

B. SSDSAR detection problem

Classical SAR (CSAR) processors assume that the target to image is a single or a set of isotropic points. These algorithms can be written as an isotropic point detector [1]. This assumption does not consider targets scattering properties. The SSDSAR algorithm sets the two following hypothesis: for each position (x, y) to image, H_0 refers to the case where the received signal, \mathbf{z} , is a white Gaussian noise \mathbf{n} , $CN(0, \sigma^2 \mathbf{I})$. H_1 corresponds to the case where the received signal is the signal scattered by a canonical element with an unknown orientation (α, β) plus \mathbf{n} . The detection problem is written as follows:

$$\begin{cases} H_0 : \mathbf{z} = \mathbf{n} \\ H_1 : \mathbf{z} = a\mathbf{s}(\alpha, \beta) + \mathbf{n} \end{cases} \quad (2)$$

where

$$\mathbf{s}(\alpha, \beta) = [\mathbf{s}_1(\alpha, \beta)^T \quad \mathbf{s}_2(\alpha, \beta)^T \quad \dots \quad \mathbf{s}_n(\alpha, \beta)^T]^T \quad (3)$$

and $\mathbf{s}_k(\alpha, \beta)$ is the signal received at position u_k , scattered by the chosen model at (x, y) with an unknown orientation α and β . The quantity a is an unknown complex attenuation coefficient. If the set spanned by $\mathbf{s}(\alpha, \beta)$ when $(\alpha, \beta) \in [0, \pi]^2$, belongs to a subspace $\langle H_{xy} \rangle$ of dimension D_H , we can rewrite the detection problem as:

$$\begin{cases} H_0 : \mathbf{z} = \mathbf{n} \\ H_1 : \mathbf{z} = \mathbf{H}_{xy}\lambda + \mathbf{n} \end{cases} \quad (4)$$

where \mathbf{H}_{xy} is an orthonormal basis ($M \times D_H$) associated to the ‘‘subspace model’’ $\langle H_{xy} \rangle$, and λ is the unknown corresponding ($D_H \times 1$) coordinate vector of the signal $a\mathbf{s}(\alpha, \beta)$.

C. CFAR Signal Subspace Detector

As the variance σ^2 is unknown, we have to develop a CFAR test fitting with this detection problem. From [4], the Generalized Likelihood Ratio (GLR) L_{SSD} can be written:

$$L_{SSD}^{1/M} = \frac{\mathbf{z}^\dagger \mathbf{P}_{\mathbf{H}_{xy}} \mathbf{z}}{\mathbf{z}^\dagger \mathbf{P}_{\mathbf{H}_{xy}}^\perp \mathbf{z}} + 1 \quad (5)$$

where $\mathbf{P}_{\mathbf{H}_{xy}}$ is the orthonormal projector onto the subspace $\langle H_{xy} \rangle$. We also have $\mathbf{P}_{\mathbf{H}_{xy}}^\perp = \mathbf{I} - \mathbf{P}_{\mathbf{H}_{xy}}$. We deduce from equation (5) that:

$$L_{SSD}^{1/M} - 1 = \frac{\|\mathbf{H}_{xy}^\dagger \mathbf{z}\|^2}{\|\mathbf{z}\|^2 - \|\mathbf{H}_{xy}^\dagger \mathbf{z}\|^2} \quad (6)$$

The basis \mathbf{H}_{xy} is deduced from the Singular Value Decomposition (SVD) of the signal matrix:

$$\mathbf{S}_{xy} = [\mathbf{s}(\alpha_1, \beta_1) \dots \mathbf{s}(\alpha_i, \beta_j) \dots \mathbf{s}(\alpha_P, \beta_Q)] \quad (7)$$

where (α_i, β_j) describe $[0, \pi^2]$.

$$\mathbf{S}_{xy} = \mathbf{U}_S \Sigma_S \mathbf{V}_S^\dagger \quad (8)$$

where \mathbf{U}_S and \mathbf{V}_S are two orthonormal matrices and Σ_S a diagonal matrix containing the singular values. \mathbf{H}_{xy}^\dagger corresponds to the D_H first singular vectors of \mathbf{U}_S associated to the D_H highest singular values.

We set the intensity of the pixel $I_{SSDSAR}(x, y)$ to:

$$I_{SSDSAR}(x, y) = \frac{\|\mathbf{H}_{xy}^\dagger \mathbf{z}\|^2}{\|\mathbf{z}\|^2 - \|\mathbf{H}_{xy}^\dagger \mathbf{z}\|^2} \quad (9)$$

III. SIGNAL OR INTERFERENCE SUBSPACE DETECTOR SAR (SISDSAR) ALGORITHM FOR DETECTION IN A FOREST

The SSDSAR algorithm has been developed to increase MMT detection probability by making assumption on the target response. No specific clutter treatment matched to the media has been considered to decrease false alarm probability: the clutter has only been modelled by a white Gaussian noise. From now on, we consider that the MMT is embedded in a forest.

A. Forest Clutter Modeling

When detection is operated on a SAR image of the forest, false alarms are mainly due to trunks response. Our treatment is based on this consideration: the forest clutter will be modelled as a trunk response plus a white Gaussian noise representing canopy response. Trunks are modelled by a cylinder of a given size tilted of an unknown angle $\delta \in [0, \delta_{max}]$ from its vertical position in a direction defined by the rotation angle $\gamma \in [0, 2\pi]$. δ_{max} is the maximum tilt angle of the trunk. Considered rotation are given in Figure 1.

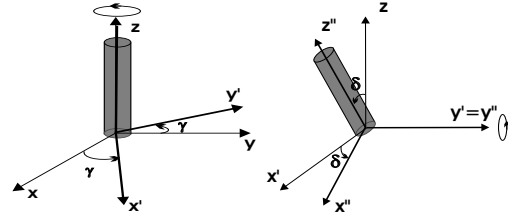


Fig. 1: Definition of the angles γ and δ

B. Detection Problem

The new two hypotheses detection problem can be described as follows: for each position (x, y) to image, H_0 refers to the case where the received signal, \mathbf{z} , is a white Gaussian noise \mathbf{n} , $CN(0, \sigma^2 \mathbf{I})$, plus the signal scattered by a vertical cylinder tilted of unknown angles (γ, δ) . H_1 corresponds to the case where the received signal is the signal scattered by a canonical element with an unknown orientation (α, β) plus \mathbf{n} . These two hypotheses implicitly set the assumption that a trunk and a MMT cannot be at the same location. From section II, we have that:

$$H_1 : \mathbf{z} = \mathbf{H}\lambda + \mathbf{n}. \quad (10)$$

From III-A:

$$H_0 : \mathbf{z} = c\mathbf{t}(\gamma, \delta) + \mathbf{n} \quad (11)$$

where $\mathbf{t}(\gamma, \delta)$ is the signal scattered by a trunk at position (x, y) , with tilt angles defined by (γ, δ) , and c a complex attenuation coefficient. As in the previous section, if:

$$\forall (\gamma, \delta) \in [0, 2\pi] \times [0, \delta_{max}], \quad \mathbf{t}(\gamma, \delta) \in \langle J_{xy} \rangle \quad (12)$$

where $\langle J_{xy} \rangle$ is a low dimensional subspace of dimension D_J defined by an orthonormal basis \mathbf{J}_{xy} , the detection problem becomes:

$$\begin{cases} H_0 : \mathbf{z} = \mathbf{J}_{xy}\mu + \mathbf{n} \\ H_1 : \mathbf{z} = \mathbf{H}_{xy}\lambda + \mathbf{n} \end{cases} \quad (13)$$

with μ and λ two unknown coordinates vectors. σ^2 , the variance of \mathbf{n} is also unknown.

C. CFAR Subspace or Interference Detector

As μ , λ and σ^2 are unknown, we replace them by their Maximum Likelihood Estimate (MLE) into the likelihood ratio to get the classical GLR L_{SISD} :

$$L_{SISD} = \frac{\max_{\sigma, \lambda \in \mathbb{C}^{D_H}} p(\mathbf{z}|H_1)}{\max_{\sigma, \mu \in \mathbb{C}^{D_J}} p(\mathbf{z}|H_0)} \quad (14)$$

For a better legibility, we set:

$$\hat{\mathbf{n}}_0 = \mathbf{z} - \mathbf{J}_{xy}\hat{\mu} \quad (15)$$

$$\hat{\mathbf{n}}_1 = \mathbf{z} - \mathbf{H}_{xy}\hat{\lambda} \quad (16)$$

where $\hat{\mathbf{n}}_0$ is the estimate of \mathbf{n} considering H_0 and $\hat{\mathbf{n}}_1$ is the estimate of \mathbf{n} considering H_1 . $\hat{\lambda}$ and $\hat{\mu}$ are the estimates of λ and μ . By using notations (15) and (16) and considering the estimates $\hat{\sigma}_1$ considering H_1 and $\hat{\sigma}_0$ considering H_0 of σ , L_{SISD} can be written as in [5]:

$$L_{SISD}^{1/M} = \frac{\|\hat{\mathbf{n}}_0\|^2}{\|\hat{\mathbf{n}}_1\|^2} \quad (17)$$

We can replace equations (15) and (16) by:

$$\hat{\mathbf{n}}_0 = \mathbf{z} - \mathbf{P}_{\mathbf{J}_{xy}}\mathbf{z} \quad (18)$$

$$\hat{\mathbf{n}}_1 = \mathbf{z} - \mathbf{P}_{\mathbf{H}_{xy}}\mathbf{z} \quad (19)$$

where $\mathbf{P}_{\mathbf{J}_{xy}} = \mathbf{J}_{xy}\mathbf{J}_{xy}^\dagger$ and $\mathbf{P}_{\mathbf{H}_{xy}} = \mathbf{H}_{xy}\mathbf{H}_{xy}^\dagger$ are two orthogonal projectors on subspaces $\langle J_{xy} \rangle$ and $\langle H_{xy} \rangle$. Finally we have:

$$L_{SISD}^{1/M} = \frac{\|\mathbf{z} - \mathbf{J}_{xy}\mathbf{J}_{xy}^\dagger\mathbf{z}\|^2}{\|\mathbf{z} - \mathbf{H}_{xy}\mathbf{H}_{xy}^\dagger\mathbf{z}\|^2} \quad (20)$$

$$= \frac{\|\mathbf{H}_{xy}^\dagger\mathbf{z}\|^2 - \|\mathbf{J}_{xy}^\dagger\mathbf{z}\|^2}{\|\mathbf{z}\|^2 - \|\mathbf{H}_{xy}^\dagger\mathbf{z}\|^2} + 1 \quad (21)$$

As in section II, the subspace basis \mathbf{J}_{xy} is obtained by SVD of the following matrix:

$$\mathbf{T}_{xy} = [\mathbf{t}(\gamma_1, \delta_1) \dots \mathbf{t}(\gamma_i, \delta_j) \dots \mathbf{t}(\gamma_{P'}, \delta_{Q'})] \quad (22)$$

$$= \mathbf{U}_T \mathbf{\Sigma}_T \mathbf{V}_T^\dagger \quad (23)$$

with (γ_i, δ_j) describing $[0, \gamma_{max}] \times [0, 2\pi]$, \mathbf{U}_T and \mathbf{V}_T two orthonormal matrices and $\mathbf{\Sigma}_T$ a diagonal matrix containing the singular values. \mathbf{J}_{xy}^\dagger corresponds to the D_J first singular vectors of \mathbf{U}_T associated to the D_J highest singular values.

We define the amplitude of the pixel $I_{SISDSAR}(x, y)$ given by the SISDSAR algorithm by:

$$I_{SISDSAR}(x, y) = \frac{\|\mathbf{H}_{xy}^\dagger\mathbf{z}\|^2 - \|\mathbf{J}_{xy}^\dagger\mathbf{z}\|^2}{\|\mathbf{z}\|^2 - \|\mathbf{H}_{xy}^\dagger\mathbf{z}\|^2} \quad (24)$$

IV. APPLICATION ON A SIMULATED FOREST

In this part, we assume that a Man Made Target (MMT) is a set of metallic plates of different sizes and orientations and trunks are tilted cylinders. The plate model has many advantages: the scattering of a metallic plate is directive, which is often a property of MMTs and it is an unusual shape in a forest (very different from the vertical cylinder we choose to model the clutter). After having simulated a metallic box response with Feko [7] (a software based on method of moments), we put it in a simulated trunk forest generated by the software COSMO [8]. Then we compare the image obtained by the CSAR, SSDSAR and SISDSAR algorithms. Performances of these algorithms are then discussed.

A. Simulation parameters

- Target Subspace model: The target subspace model is generated with a $1 \text{ m} \times 2 \text{ m}$ metallic plate. The code used for the computation of the signal scattered by the plate is based on the physical optics approximation, which requires that its dimensions are larger than the wavelength. The scattering matrix of a perfectly conducting plate used to compute scattered signals is derived from [6].
- Interference Subspace model: The Interference Subspace model is generated with a 10 m high cylinder with a 25 cm radius, $\delta_{max} = 10^\circ$.
- Configuration of the simulated forest: trunks are 11 meters high and have a radius of 19 centimeters. They are separated one from others with a mean distance of 7 meters (more or less 1 meter). Trunks are tilted of an angle between 0 and 2 degrees (worst case). Interactions between the target and trunks are neglected. The scene coordinates are: $x = [90, 150]$ m and $y = [-25, 20]$ m.
- Target Model: we consider the $2\text{m} \times 1.5\text{m} \times 1\text{m}$ metallic parallelepiped, tilted of a $\pi/9$ angle around axis \mathbf{z} , lying on a perfectly conducting (PEC) ground, located at $(118, -1)$.
- Flight configuration and sampling: starting at $u_0 = -50$ m, ending at $u_{200} = 50$ m, $\delta_u = 0.5$ m. Flight height is 100 m. We are in a far field configuration.
- Emitted chirp: the central frequency of the chirp is 400 MHz with a bandwidth of 100 MHz. We only consider VV polarization.

B. Low dimensional subspace hypothesis

As said previously, we assumed that both the target model (plates) and the interference model (trunks) generated a low dimensional subspace. The subspace generated by the plate as already been demonstrated to be low dimensional [1]. Figure 2 represents the singular values of \mathbf{T}_{xy}

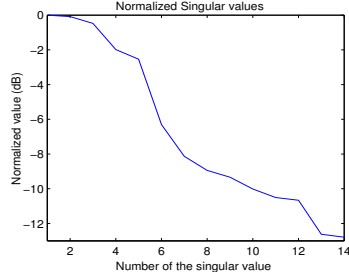


Fig. 2: Normalized Singular values associated to the cylinder subspace

If we consider that the last relevant singular value is at 10 dB from the maximum one, the trunk subspace has 12 dimensions. The generated subspace can be considered as a low dimensional subspace.

C. Application of the algorithms

The three different algorithms, CSAR, SSDSAR and SISDSAR are applied to generate the image of the scene described previously. Results are plotted respectively in Figures 3, 4 and 5. The target is pointed on each image by a small arrow. The improvement between the CSAR image and the two other images is clear. From Figure 3 to Figure 4, the magnitude of pixels corresponding to the target is significantly increased and becomes higher than the trunks one. From Figure 4 to Figure 5, the magnitude of the target is kept at the same level, while the magnitude of trunks significantly decreases.

If we consider the number of false alarms pixels on the images versus a threshold (Figure 6), the difference between the two images is easier to quantify.

V. CONCLUSION

This article developed two new CFAR methods to increase MMT detection performance. One was directly derived from a previous work based on simple assumptions on the MMT electromagnetic scattering properties. The other focused on decreasing the forest clutter: a new signal or interference subspace detector has been developed where interferences are modelled by a cylinder subspace. Results obtained are encouraging and tests on real data will be proceeded.

REFERENCES

- [1] R. Durand, G. Ginolhac, P. Forster, L. Thirion, *New SAR processor based on a Subspace Detector*, EUSIPCO 2006, Florence, Italy, September 2006.
- [2] R. Durand, L. Thirion, G. Ginolhac, P. Forster, *Man Made Target Detection in a Forest with a Subspace Detector SAR Processor*, IGARSS 2006, Denver, USA, August 2006
- [3] R. Durand, G. Ginolhac, P. Forster, L. Thirion, *Implementation and Optimization of a SAR Processor Based on a Subspace Detector. Application to Man Made Target Detection in a Forest*, International SAR and SAS Conference 2006, Lerici, Italy, September 2006
- [4] L.L.Scharf, *Statistical Signal Processing: Detection, Estimation and Time Series Analysis*. Addison-Wesley Publishing Co., 1990.
- [5] L.L.Scharf, B.Friedlander, *Matched Subspace Detector*, IEEE Transactions on Signal Processing, vol.42, n^o8, August 1994.

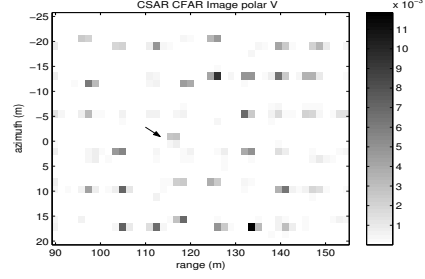


Fig. 3: CSAR image

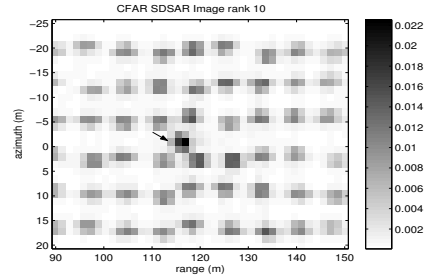


Fig. 4: SSDSAR image

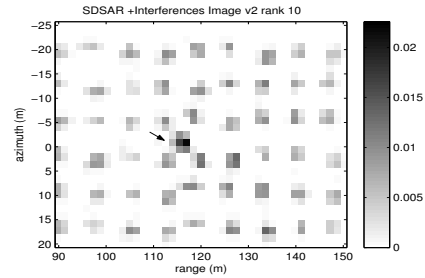


Fig. 5: SISDSAR image

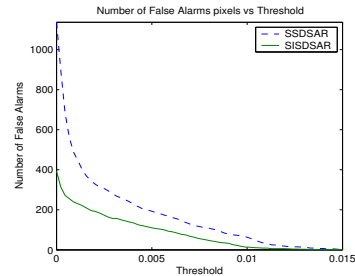


Fig. 6: Number of false alarms vs threshold

- [6] F.T. Ulaby, C. Elachi, *Radar Polarimetry for Geoscience Applications*. F.T.Ulaby, C.Elachi Editors, 1990.
- [7] *Feko, User's Manual*, EM Software and System, June 2004
- [8] L.Thirion, E.Colin, C.Dahon, *Capabilities of a forest coherent scattering model applied to radiometry, interferometry and polarimetry at P and L-band*, IEEE TGRS, vol.44, n.4, April 2006, pp 849-862.